Mineralogical Effects on Elastic Properties and Anisotropies of Organic Shales

Xuan Qin*, De-hua Han, Fuyong Yan, and Luanxiao Zhao, Rock Physics Lab, University of Houston

Summary

In this study, we investigate the reported ultrasonic measurements of core samples of organic shale and our lab measurements. We focus on Vp/Vs ratios, P-impedance, and velocity anisotropies for different types of organic shales. A layered model is constructed to explain why the silica-rich shales tend to have higher S-wave anisotropy and calcareous shales tend to have higher P-wave anisotropy. The modeling results of the ratio of Thomsen's anisotropic parameters, γ / ε, remain approximately as constants in the silica-rich and calcareous shales. Hence, γ / ε ratio may be potentially treated as an indicator for mineralogical composition in shale reservoirs. We also observe linear trends between Thomsen's parameters, ε and δ, in the calcareous shale. Additionally, ν_{12} and ν_{31}, Poisson's ratios in a transverse isotropic (TI) medium, exhibit a linear relationship in silica-rich shales and clay-rich shales, providing insights for characterizing mineralogical composition of organic shales.

Introduction

North American unconventional shale plays gain extensive attention in recent years. Although we extract gas from these so-called "shales", clay minerals are not generally dominated in these formations. The solid phase of organic shale is complicated and normally composed of a variety of materials, such as clay minerals (smectite, illite, chlorite, kaolinite, etc.), non-clay silicate minerals (quartz, feldspar, plagioclase, etc.), carbonate minerals (calcite, ankerite, siderite, dolomite, etc.), and other minerals like pyrite, etc. It is meaningful to study the mineralogical effects on the properties of organic shale, because this is closely related to the seismic signature and fracability of the shale reservoirs.

Mineralogical constituents can be sourced from terrigenous material, including siliciclastic minerals (clay minerals, quartz, feldspars, and rock fragments), biogenic components, containing calcite and silica minerals, and diagenetic products, such as pore-filling carbonate cement, pyrite framboids, silica, and clay minerals (Hart et al., 2013). Based on the mineralogical compositions, shale plays can be divided into three types, i.e. silica-rich shale, calcareous shale, and clay-rich shale. The Triassic-Jurassic boundary can play a key role in dividing the threshold of potentials of forming silica-rich or calcareous shale, because before the Jurassic period, planktonic organisms produce less calcium carbonate than silica (Hart et al., 2013). Moreover, we observe that clay-rich shale plays are

less common than the other two types, and the mineralogical compositions of shale plays are generally dominated by biogenic quartz or calcite, or mixtures of them that can be present as fine-grained detritus and cement components. So rock physics models developed for clay-dominated mudstones are inappropriate and cannot be applied to organic shale. Figure 1 shows several shale reservoirs and their major mineralogical composition types plotted in the ternary diagram, where three vertices represent one of the three kinds of minerals reaching the highest amount. Different colors represent mineralogical components in the Eagle Ford, Marcellus, Woodford, Horn River, Haynesville, and Wealden shales. For example, the Eagle Ford reservoir rock (blue area) is well-known for its calcareous richness. Other unconventional plays, such as the Marcellus (red area), Haynesville (yellow area), etc., also contain large amounts of calcareous compositions. The Woodford shale (black area) is generally composed of quartz, illite, chlorite, dolomite, and pyrite, but its quartz volume is dominant (Abousleiman et al., 2007).
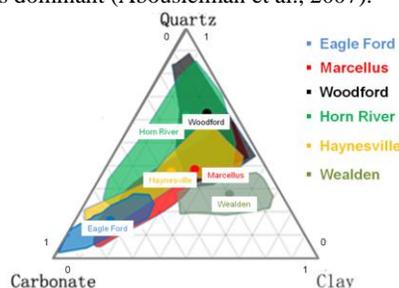

Figure 1. Some shale plays and their classifications based on mineralogical types (Modified from Passey et al., 2010).

Mineralogical effects on elastic properties

We collect core data of organic shale from several authors' work (Johnston and Christensen, 1995; Vernik and Liu, 1997; Jakobsen and Johansen, 2000; Abousleiman et al., 2007; Karastathis, 2007) and core data measured by us (RPL), which are summarized in Table 1. Mineralogical effects on Vp/Vs ratios (normal-to-bedding P- and S-wave velocities) and P-impedance of organic shales are investigated based on their mineralogical types (Figure 2).

In Figure 2, data denoted with the blue dashed points are samples of the clay-rich shales from north Texas (Karastathis, 2007), with an average weighted mineralogical composition of 35% clay, 31% quartz, and 17% carbonate, and the North Sea Shale (Jakobsen and Johansen, 2000). Data denoted with the yellow circles are the silica-rich shales, from the Woodford (Abousleiman et

SEG International Exposition and 86th Annual Meeting

al., 2007), North Sea (Jakobsen and Johansen, 2000), Chattanooga, New Albany, and Antrim Shale (Johnston and Christensen, 1995). For example, the average mineralogical compositions of the Woodford shale, by volume, are 41.1% silica, 6.5% carbonates, 29.9% clay, and 14.7% kerogen, with some other minor ($< 7.8\%$) minerals such as pyrite. The green squares indicate calcareous shale samples from the Woodford (Vernik and Liu, 1997), North Sea (Jakobsen and Johansen, 2000) as well as the Haynesville and Eagle Ford shale measured in our lab.

Table 1. Ultrasonic measurements of organic shale samples used in this study.

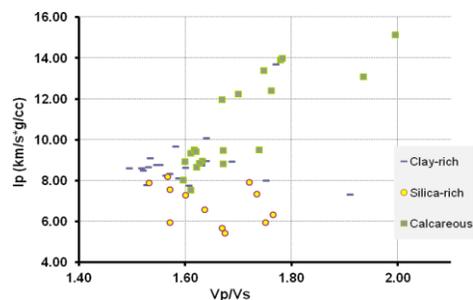| Mineralogy Types	Sample Numbers	Shale Formations
Silica-rich	12	Woodford(5), North Sea(1), Chattanooga(2), New Albany(3), and Antrim(1)
Clay-rich	21	North Texas(18) and North Sea(3)
Calcareous	20	Haynesville(12), Eagle Ford(6), North Sea(1), and Woodford(1)

Figure 2. P-impedane vs. Vp/Vs ratio for clay-rich (blue), sillica-rich (yellow), and calcareous shales (green).

The Vp/Vs ratios of clay-rich shale samples range from 1.5 to 1.91 and the Vp/Vs ratios of silica-rich shales range from 1.53 to 1.77, and Calcareous shales have Vp/Vs ratios ranging from 1.6 to 2.0. The Vp/Vs ratios for calcareous shales are higher than those of the other two types. Lower Vp/Vs ratios in silica-rich shales are mainly due to the existence of large amount of quartz. Since the shear modulus of quartz is 44 GPa and is higher than its bulk modulus at 37 GPa, such a low K/μ ratio explains the low Vp/Vs ratio of silica-rich. Several silica-rich shales from the Woodford formation contain higher porosities (17.2% on average) than clay-rich shales from north Texas (6.2% on average). Increasing porosity decreases Vp and Vs, but Vs decreases more rapidly, which can be inferred from Han's empirical relations (Han et al., 1986): for dry shaly sandstone at 40 MPa,

$$V_p = 5.41 - 6.35\phi - 2.87C , \qquad (1)$$

$$V_s = 3.57 - 4.57\phi - 1.83C , \qquad (2)$$

and for water-saturated shaly sandstone at 40 MPa,

$$V_p = 5.59 - 6.93\phi - 2.18C , \qquad (3)$$

$$V_s = 3.52 - 4.91\phi - 1.89C , \qquad (4)$$

where ϕ is porosity, and C is clay volume fraction. High porosities account for the low P-impedance of these silica-rich shales. Although clay-rich formations are characterized with relative high Vp/Vs ratios, with equations (1) and (2), we can theoretically derive a "dry clay point" with a Vp/Vs ratio of 1.46, which implies that the Vp/Vs ratio of the dry clay exhibits the similar behavior of quartz. Meanwhile, we also note a "wet clay point" from equations (3) and (4), which has a Vp/Vs ratio as high as 2.09. Bound water exists between the clay platelets (especially smectite), which is considered to be responsible for the low shear modulus of clay. Hence, the clay properties are strongly dependent on its water content, which can change its Vp/Vs ratio significantly. Both the Vp/Vs ratio and P-impedance of calcareous shales are overall higher than those of clay-rich and silica-rich shales. Calcite minerals have a density of 2.71 g/cc, a bulk modulus of 76.8 GPa, and shear modulus of 32 GPa (Mavko et al., 2009). Thus, increasing the carbonate content can increase the Vp/Vs ratio and P-impedance. However, some calcareous shales have Vp/Vs ratios close to 1.6, and this is likely due to the calcite cementation formed in the shale matrix. When the in-situ temperature increases, organic matter can be cooked. If the shale's permeability is too low to allow byproducts, such as CO_2 and water, to run out in time, it will finally lead to the precipitation of calcite. Cementation generally decreases the rock's Vp/Vs ratio, since cement materials between mineral grains can significantly enhance the rock's resistance to shear deformation.

Mineralogical effects on anisotropies

The properties of shales change vertically (at centimeter scale) much faster than they do laterally (at dekameter scale). Figure 3 plots P-wave anisotropy (ε) and S-wave anisotropy (γ) for clay-rich shales (blue dashed points), sillica-rich shales (yellow circles), and calcareous shales (green squares). Overall speaking, these data points show an approximately linear trend with a slope of 1 to describe P- and S-wave anisotropies. Their individual linear regression equations are shown in Figure 3. Specifically, for calcareous shales, the linear approximation has the highest correlation coefficient, $R^2 = 0.9506$, thereby ε and γ are almost equal. Among sillica-rich shale samples, γ is normally larger than ε with $R^2 = 0.9066$. Among clay-rich shale samples, γ is normally less than ε with the poorest correlation. All these trend features of different mineralogical contents can provide us with insights on organic shales mineralogy studies.
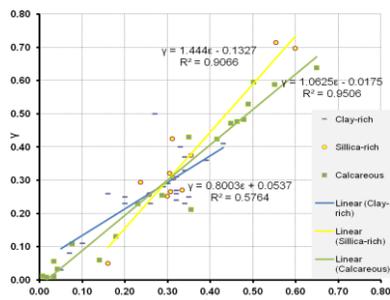
Figure 3. P-wave anisotropy ε vs. S-wave anisotropy γ for clay-rich (blue), sillica-rich (yellow), and calcareous shales (green). Blue, yellow, and green lines are the linear fits for clay-rich, silica-rich, and calcareous shales, respectively.

The Voigt and Reuss bounds are applied to interpret the relationship between the P-wave and S-wave anisotropies of the three types of organic shales. Shale samples are assumed to be composed of layers of pure clay and pure quartz/calcite, which is used to simulate silica-rich/calcareous shale. The Voigt bound simulates the iso-strain case, in which the effective moduli are the largest when the compositions and volume fractions of the multi-phase composites are determined. Therefore, the highest P- and S-wave velocities can be simulated, which propagate parallel to the bedding plane. The Reuss bound is the lower bound of the moduli or velocities when the compositions and volume fractions of the multi-phase composites are determined. It simulates the iso-stress case, which corresponds to the case when the waves travel normal to the bedding plane.

We set up simple layer models as follows: quartz or calcite volume fraction varies from 50% to 80% in silica-rich or calcareous shale model and clay is the remaining composition. We can calculate the Voigt and Reuss bounds in these two types of organic shales and thus the P- and S-wave anisotropies denoted with Thomsen's parameters, ε and γ.

The three minerals are treated as isotopic materials. For example, quartz has a bulk modulus of 37 GPa, a shear modulus of 44 GPa, and a grain density of 2.65 g/cc; calcite has a bulk modulus of 76.8 GPa, a shear modulus of 32 GPa, and a grain density of 2.71 g/cc; clay has a bulk modulus of 25 GPa, a shear modulus of 9 GPa (Han et al., 1986) and a grain density of 2.55 g/cc. Figure 4 demonstrates that for silica-rich shale model, γ/ε ratio is close to 2; with an increase of quartz volume ($V_{quartz} > $ 50%), γ/ε ratio remains approximately constant and values of ε and γ gradually decrease. This provides an explanation from the perspective of intrinsic anisotropy due to mineralogical properties of why γ is larger than ε in

silica-rich shales. For calcareous shales, with an increase of calcite content ($V_{calcite} > $ 50%), γ/ε ratio remains as a constant of 1.19 and values of ε and γ gradually decrease. We also notice that when quartz volume varies from 50% to 60%, the trend is not linear due to the large shear modulus of quartz. Therefore, we argue that silica-rich shales have larger γ/ε than calcareous shales. The constant γ/ε ratios in silica-rich and calcareous shales may be used as a mineralogical composites indicator, and our future work can be put more emphasis on the upscaling of anisotropy from core plugs to seismic resolution.
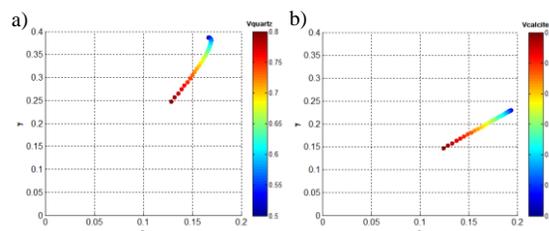

Figure 4. P-wave and S-wave anisotropies for (a) the silica-rich and (b) calcareous shales models, which are color-coded with the volume fractions of quartz and calcite.

Moreover, we notice that in the rock physics modeling, when the volume fraction of quartz in the silica-rich shale equals to the volume fraction of calcite in the calcareous shale, silica-rich shale has lower P-wave anisotropy but higher S-wave anisotropy than calcareous shale. This is because Voigt bound uses an arithmetic mean to calculate the effective bulk and shear moduli, which determines the largest P- and S-wave velocities but is rare for real rocks. Likewise, Reuss bound uses a harmonic mean to calculate the effective bulk and shear moduli, which determines the lowest P- and S-wave velocities and is suitable for rock in suspension. Therefore, this method gives the largest ε and γ when we only consider the anisotropy induced by the layer medium intrinsically. The bulk modulus's difference between calcite (76.8 GPa) and clay (25 GPa) is larger than that between quartz (37 GPa) and clay, and thus, we suggest that calcareous shales contain higher P-wave anisotropy. The shear modulus's difference between quartz (44 GPa) and clay (9 GPa) is larger than that of calcite (32 GPa) and clay, and consequently, the silica-rich shales contain higher S-wave anisotropy.

Thomsen's anisotropic parmeter, δ, one of the most important parameters to determine the NMO velocity in a TI medium, is determined by the difference between the P-wave and SV-wave anisotropies of the medium (Thomsen, 1986). However, the physical meaning of δ remains to be explored. In Figure 5, there can be a linear trend to describe ε and δ behavior for calcareous shales, which suggests that we can refer to such a correlation or constraints when

studying calcareous shale. However, it is unreliable to derive a linear relation for silica-rich and clay-rich shales due to the scattered points in ε - δ plane.
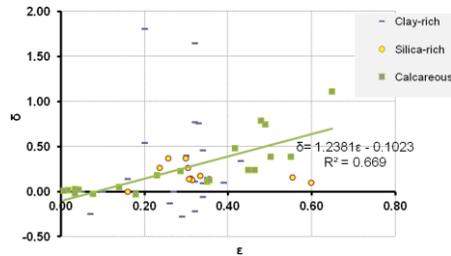

Figure 5. Thomsen's anisotropic paramters ε vs. δ for clay-rich (blue), silica-rich (yellow), and calcareous shales (green). The green line is the linear fit for calcareous shales.

For a TI medium, we can use three Poisson's ratios (Mavko et al., 2009) to study anisotropic material. ν_{31} is the negative ratio of strain (ε_{11}) parallel in the bedding plane to the strain (ε_{33}) along the symmetry due to the uniaxial stress along the symmetry, and ν_{12} is the negative ratio of strain (ε_{22}) in the bedding and normal to the stress to the strain (ε_{11}) in the bedding plane and along the stress:

$$\nu_{31} = -\frac{\varepsilon_{11}}{\varepsilon_{33}} = \frac{C_{13}}{C_{11}+C_{12}}, \qquad (5)$$

$$\nu_{12} = -\frac{\varepsilon_{22}}{\varepsilon_{11}} = \frac{C_{12}C_{33}-C_{13}^2}{C_{11}C_{33}-C_{13}^2}, \qquad (6)$$

where C_{ij} refers to elastic stiffnesses.

Figure 6 displays the relation between ν_{12} and ν_{31} for clay-rich, silica-rich, and calcareous shales. ν_{31} decrease with increasing ν_{12} as a whole. We can use good linear approximations to describe the behavior between ν_{12} and ν_{31} for clay-rich shale and silica-rich shales. All of ν_{31} values of these samples are positive, but ν_{12} of clay-rich and calcareous shales can be negative, which means when we apply uniaxial stress along the shale bedding, the strain along the stress and normal to the stress in the bedding plane have the same direction, but the strain along the symmetry has a reverse sign and a relative large magnitude to the other two. When we go back and check the samples

with negative ν_{12}, their δ parameters are all larger than 0.5. Hence, Poisson's ratios in the TI medium can provide us strategies when studying rock anisotropy and geomechanical properties. The relationships between ν_{12} and ν_{31} in silica-rich and clay-rich shales enlighten us on lithology analysis of organic shales.
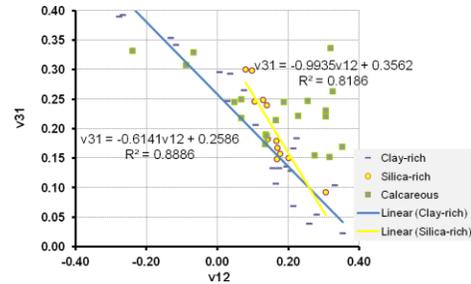

Figure 6. Poisson's ratios ν_{12} vs. ν_{31} for clay-rich, sillica-rich, and calcareous shales. The blue and yellow lines are the linear fits for clay-rich shales and silica-rich shales, respectively.

Conclusions

To study the mineralogical effects on Vp-Vs relations and velocity anisotropies of organic shales, we have analyzed the ultrasonic measurements of the three types of organic shales: silica-rich shales, clay-rich shales, and calcareous shales. Silica-rich shales generally have low Vp/Vs ratios varying from 1.53 to 1.77, clay-rich shales' Vp/Vs ratios have a large range from 1.5 to 1.91, which are dependent on the amount of water in the clay minerals, and calcareous shales have Vp/Vs ratios ranging from 1.6 to 2.0, which rely on the constituents of detrital (terrigenous) or diagenetic (cement) mineral. The P-wave and S-wave anisotropies correlate linearly in these three types of organic shales. However, silica-rich shales generally have the largest γ/ε ratios. The Voigt and Reuss bounds are used to explain why the silica-rich have larger S-wave anisotropy but lower P-wave anisotropy than calcareous shales, which are accorded with the collected core measurements. The δ/ε ratio approximately remains as a constant once the mineralogical composites are determined, which may be used as a lithology indicator. Correlations between δ and ε and ν_{12} and ν_{31} can potentially provide insights on characterizing calcareous, clay-rich, and silica-rich shales.

Acknowledgements

REFERENCES

Abousleiman, Y., M. Tran, S. Hoang, C. Bobko, A. Ortega, and F. Ulm, 2007, Geomechanics field and
laboratory characterization of the Woodford Shale: The next gas play: SPE Annual Technical
Conference and Exhibition, SPE 110120.

Han, D., A. Nur, and D. Morgan, 1986, Effects of porosity and clay content on wave velocities in
sandstones: Geophysics, **51**, 2093–2107, http://dx.doi.org/10.1190/1.1442062.

Hart, B., J. Macquaker, and K. Taylor, 2013, Mudstone (shale) depositional and diagenetic processes:
Implications for seismic analyses of source-rock reservoirs: Interpretation, **1**, B7–B26,
http://dx.doi.org/10.1190/INT-2013-0003.1.

Jakobsen, M., and T. A. Johansen, 2000, Anisotropic approximations for mudrocks: A seismic laboratory
study: Geophysics, **65**, 1711–1725, http://dx.doi.org/10.1190/1.1444856.

Johnston, J., and N. Christensen, 1995, Seismic anisotropy of shales: Journal of Geophysical Research,
100, 5991–6003, http://dx.doi.org/10.1029/95JB00031.

Karastathis, A., 2007, Petrophysical measurements on tight gas shale: Ph.D. dissertation, University of
Oklahoma.

Mavko, G., T. Mukerji, and J. Dvorkin, 2009, The rock physics handbook: Cambridge University Press.

Passey, Q. R., K. M. Bohacs, W. L. Esch, R. E. Klimentidis, and S. Sinha, 2010, From oil-prone source
rock to gas-producing shale reservoir-geologic and petrophysical characterization of
unconventional shale gas reservoirs: International Oil and Gas Conference and Exhibition in
China.

Thomsen, L., 1986, Weak elastic anisotropy: Geophysics, **51**, 1954–1966,
http://dx.doi.org/10.1190/1.1442051.

Vernik, L., and X. Liu, 1997, Velocity anisotropy in shales: A petrophysical study: Geophysics,
62, 521–532, http://dx.doi.org/10.1190/1.1444162.